Transonic Wave Drag Estimation and Optimization Using the Nonlinear Area Rule

N. Malmuth*
Rockwell International, Thousand Oaks, California
C. C. Wu†
University of California, Los Angeles, California
and
J. D. Cole‡
Rensselaer Polytechnic Institute, Troy, New York

Nonlinear area ruling procedures based on the transonic slender body and lift-dominated theories are described as a means of providing low-cost wave drag estimates and optima for basepoint definition. The computational implementation is capable of accurately predicting drag rise of realistic configurations and shows applicability to moderate supersonic Mach numbers. An analogy between the zero-lift and lift-dominated case establishes a basis for sizeable wave drag due to lift reduction through planform and sectional shaping. Results illustrating the potential benefits are shown for a fighter configuration in which a small movement of the maximum thickness location of the equivalent body of revolution with the volume fixed gives a fourfold reduction in zero-lift wave drag. This benefit can be translated into similar reductions in transonic wave drag due to lift.

Introduction

THERE is a continuing need for rapid turnaround and conceptual methods for the design synthesis of fighter configurations that exploit nonlinear aerodynamic phenomena. This is particularly true for missions that involve a compromise between the transonic maneuver point and supersonic cruise conditions. To achieve such agility and energy maneuverability attributes as the high rate of climb and acceleration necessary for survivability against transonic threats, low drag levels are essential. Because of the steepness of the wave systems, the presence of mixed flow conditions, as well as shock phenomena, nonlinear effects are a crucial factor. For design optimality, these phenomena should be considered for the basepoint definition. Current approaches such as that of Ref. 1 use linear methods for this first step of the configuration development cycle in conjunction with computational fluid dynamics (CFD) codes for subsequent refinements. An alternate approach would develop the basepoint arrangement from *nonlinear* aerodynamic considerations. A cogent concern at this stage is the minimization of transonic shock drag in relation to vortex drag. Linear methods are not equipped to deal with these issues.

In this paper, nonlinear area ruling procedures based on transonic slender-body theory will be described as a means of providing reliable, low-cost, conceptual wave drag estimates and optima useful for basepoint design.

Earlier effort by Oswatitsch and Keune,[2] Heaslet and Spreiter,[3] and Cole[4] provided the analytical foundations of the equivalence and area rules basic to the studies to be described in this paper. The area rule developed in these analyses gave a method from which the transonic zero-lift wave drag could be computed from that of an equivalent body of revolution (EBR). This formulation is a nonlinear counterpart to the Whitcomb,[5] Jones[6] linear area rule methodology used by industry for many years in conceptual design.

Cheng and Hafez,[7] Cheng,[8] Cramer,[9,10] as well as Barnwell[11] and, most recently, Cole,[12] have treated lifting effects in the equivalence rule and transonic slender body theory. *What has been virtually untapped is the tremendous potential of a computational procedure based on the nonlinear area rule to reduce sizeably wave drag levels and maximize aerodynamic efficiency.*

Initial studies along these lines based on a "parameterized inverse method" were reported in Ref. 13. These indicated that shock drag of bodies of revolution could be virtually eliminated by nullifying the jump discontinuity in the surface pressure distribution associated with a shock. This calculation was achieved by reshaping of the body contour and hints at a positive answer to the fundamental question concerning the existence of shock-free axially symmetric bodies in transonic flow. Such an issue is of great significance to aerodynamic design, since these bodies can be thought of as EBR's representative of complete airplane configurations.

The parameterized inverse method of Ref. 13 has the advantage that it often provides a close connection to drag reduction because of its direct connection to the shock pressure discontinuities. Frequently, however, shock envelopes form off the body and no pressure discontinuities occur on it. In this paper, another procedure will be outlined to deal with such situations. It considers the zero-lift wave drag as a payoff functional of the EBR shape that is computed from the solution of the boundary value problem of the transonic small-disturbance equation. A procedure for optimizing this functional will be illustrated for a fighter configuration. Prior to this example, application of the method in establishing useful wave drag estimates will be demonstrated for configurations ranging from simple shapes to realistic arrangements. For the latter, a set of similar validations were performed by Sedin[14] in a different context. Agrell et al.[15] studied the limitations of the equivalence rule

Presented as Paper 86-1798 at the AIAA 4th Applied Aerodynamics Conference, San Diego, CA, June 9-11, 1986; received July 21, 1986; revision received Nov. 19, 1986.

*Member of Technical Staff, Science Center. Associate Fellow AIAA.
†Associate Research Physicist.
‡Professor. Fellow AIAA.

in connection with not-so-slender configurations. Chan[16] and Sedin[14] investigated experimental confirmation of the modification of the area rule due to lift proposed by Cheng and Hafez[7] as well as Barnwell.[11]

In the last portion of this paper, a computational implementation of a new asymptotic method for the treatment of the lift effect on wave drag more fully described in Ref. 12 will be illustrated. Its consequences with respect to optimization will be briefly discussed.

Zero-Lift Theory

For purposes of this discussion, the transonic area rule results given in Ref. 4 will be summarized.

Considering the coordinate system shown in Fig. 1, a class of slender bodies given by

$$B=r-\delta F(x,\theta)=0$$

$$r^2=y^2+z^2,\ \theta=\tan^{-1}z/y \tag{1}$$

in transonic flow, transonic small disturbance theory is based on the limit process

$$\delta\to 0,\ K=\frac{1-M_\infty^2}{\delta^2}\ \text{fixed} \tag{2}$$

where M_∞ is the freestream Mach number; U, P_∞, and ρ_∞ the freestream speed, pressure, and density; and δ a dimensionless parameter related to the lateral extent of the body. Matching considerations show that, in an outer region which preserves the structure of the Mach waves, the flow relaxes to axial symmetry to dominant order. To keep the Mach wave structure fixed, the coordinate straining $\tilde{r}=\delta r$ fixed in the limit [Eq. (2)] is used. In this limit, the body shrinks to the axis $\tilde{r}=0$, $0<x<1$, and the asymptotic expansion for the velocity potential Φ is

$$\frac{\Phi}{U}=x+\delta^2\phi(x,\tilde{r};K)+\ldots \tag{3}$$

Substitution of Eq. (3) into the exact equations gives the transonic small-disturbance boundary value problem

$$[K-(\gamma+1)\phi_x]\phi_{xx}+\frac{1}{\tilde{r}}(\tilde{r}\phi_{\tilde{r}})_{\tilde{r}}=0 \tag{4a}$$

$$\lim_{\tilde{r}\to 0}\tilde{r}\phi_{\tilde{r}}=\mathcal{S}(x) \tag{4b}$$

for the perturbation potential ϕ, where by matching to dominant orders with an inner expansion for the body near field

$$\mathcal{S}(x)=\frac{1}{2\pi}A'(x) \tag{5a}$$

$$A=\frac{1}{2}\int_0^{2\pi}F^2\mathrm{d}\theta=\text{cross-sectional area}$$

$$=\pi F^2\ \text{for axially symmetric bodies} \tag{5b}$$

The inner region is harmonic in cross-flow planes and has a characteristic length scale equal to δ. These results can be obtained by direct matching between the inner and outer regions.

However, an analysis given in Ref. 17 has shown that an intermediate expansion is needed to provide the correct matching to higher orders.

In accord with Eq. (4b) and the basic source-like character of the far field of the inner solution (even with moderate lift), the expansion of ϕ near $r\to 0$ is

$$\phi(x,\tilde{r},K)=\mathcal{S}(x)\log\tilde{r}+g(x;K)+\mathcal{O}(\tilde{r}^2\log^2\tilde{r}) \tag{6}$$

where $g(x;K)$ is the essential unknown part of the pressure distribution connected to the wave drag.

Application of the momentum theorem to a cylindrical control surface enclosing the inner region gives the drag D as

$$\frac{D}{\rho_\infty U^2}=-\delta^4\log\delta\frac{[A'(1)]^2}{2\pi}+\delta^4\left[-A'(1)g(1)\right.$$

$$\left.-\frac{1}{2}\oint_{C_B}\phi_2^*\frac{\partial\phi_2^*}{\partial n}\,\mathrm{d}l+\int_0^1 A''(x)g(x)\mathrm{d}x\right] \tag{7}$$

In Eq. (7), the line integral is taken around a contour C_B defined by the line $r=F(1,\theta)$, representing the shape of the body's tail. The quantity $\phi_2^*=\phi^*-g$ at $x=1$, where ϕ^* is a term in the inner expansion. Thus, if Φ is the velocity potential, its inner expansion is

$$\frac{\Phi}{U}=x+(\delta^2\log\delta)2S^*(x)+\delta^2\phi(x,r^*,\theta)+\ldots$$

$$K,r^*=r/\delta\ \text{fixed as}\ \delta\to 0 \tag{8}$$

Returning to the line integral in Eq. (7), ϕ_2^* solves the cross-flow boundary value problem shown schematically in Fig. 2, where Δ signifies the Laplacian and $\partial/\partial n$ indicates differentiation in the outward normal direction to C_B.

The contour integral is the only term in Eq. (7) which involves details of the cross-sectional shape. When it vanishes, we have the area rule. This occurs if

$$1)\ F_x(1,\theta)=0\ \text{and}\ 2)\ F(1,\theta)=0$$

and only the last term remains in Eq. (7). If

$$3)\ FF_x=\text{const}\ (C_B\ \text{axisymmetric})$$

then only the line integral vanishes in Eq. (7).

It is of interest to explore the moderate supersonic limit of Eq. (7) associated with $K\to-\infty$. This gives

$$\frac{D}{\rho_\infty U^2}=-(\delta^4\log\delta)\frac{[A'(1)]^2}{2\pi}$$

$$+\frac{\delta^4}{2\pi}\left\{-\frac{[A'(1)]^2}{2}\log\sqrt{\frac{|K|}{2}}\right.$$

$$+\int_0^1 A''(x')\log(1-x')\mathrm{d}x'$$

$$-\int_0^1 A''(x)\mathrm{d}x\int_0^x A''(x')\log(x-x')\mathrm{d}x'$$

$$\left.-\frac{1}{2}\oint_{C_B}\phi_2^*\frac{\partial\phi_2^*}{\partial n}\mathrm{d}l\right\} \tag{9}$$

Equation (9) is close to the von Kármán integral formula (cf. Refs. 18-20), differing only by an additive constant, i.e.,

$$D_{\text{Eq. (9)}}=D_{\text{von Kármán integral}}$$

$$-(\delta^4\log\delta)\frac{[A'(1)]^2}{4\pi}\rho_\infty U^2 \tag{10}$$

This difference is presumably associated with a residual nonlinear behavior of the transonic theory in the $K\to-\infty$ limit as compared to the supersonic slender body theory

from which von Kármán's formula is derived. A study of $K \to \pm\infty$ asymptotics embedded within transonic small disturbance theory is needed to clarify this phenomenon. The consequences of Eq. (10) will be indicated in the Results section.

Lift Effects

Limit process expansions of the type used in the previous sections have been applied to treat transonic shock drag due to lift. This theory has been detailed in Ref. 12. For purposes of this paper, only the main results will be indicated.

In contrast to the previous section, a pointed winglike shape such as that depicted in Fig. 3 will be considered. The focus will be the "lift-dominated" transonic case, i.e., when the lift is so large that it produces significant wave drag. For simplicity, the discussion will be initially limited to zero thickness, twisted and cambered wings. Some remarks will be made subsequently regarding incorporation of wing thickness and body effects.

Referring to Fig. 3, a pointed wing is shown in relation to wind (x,y,z) and body (x',y',z) axes. A distinguished limit will be considered for which lift production gives a nonlinear source-like flow directly analogous to the zero-lift case. This source flow generates wave drag.

Denoting the body shape function as $B'(x',y',z)$ then

$$B' = y' - \tau c(x',z) = 0 \tag{11}$$

where τ is a gauge function ordering the camber and twist in relation to the angle of attack α and c the wing camber-twist distribution. If b = semispan, distinguished limits for the near- and far-field flow are defined, in which

$$K = \frac{1-M_\infty^2}{\epsilon_1(\alpha)}, \quad T = \frac{\tau}{\alpha}, \quad b \text{ fixed as } \alpha \to 0 \tag{12}$$

with $\epsilon_1(\alpha)$ a gage function to be determined by matching. We anticipate that the incidence α associated with significant wave drag due to lift will be numerically of the order encountered in transonic maneuver scenarios, i.e., $\alpha \approx 10$ deg.

Initially omitting switchback terms, the inner (near-field) expansion for the velocity potential in the limit of Eq. (12) is assumed to be

$$\frac{\Phi(x,y,z;\, M_\infty,\alpha)}{U} = x + \alpha\varphi_1(x,y,z;\, K) + \alpha^2\varphi_2 + \ldots \tag{13}$$

In accord with the previous discussion, a central problem is the determination of the behavior of φ_1 and φ_2 near the point at infinity. Substitution of Eq. (13) into the exact equations and boundary conditions and retaining terms to the indicated orders leads to the following boundary value problems for these quantities:

$$\mathcal{O}(\alpha):\ \Delta\varphi_1 \equiv \varphi_{1yy} + \varphi_{1zz} = 0 \tag{14a}$$

$$\varphi_{1y}(x,0,z) = -1 + Tc_x(x,z) \tag{14b}$$

$$\mathcal{O}(\alpha^2):\ \Delta\varphi_2 = (\gamma+1)\varphi_{1x}\varphi_{1xx} + (\varphi_{1y}^2 + \varphi_{1z}^2)_x \tag{15a}$$

$$\varphi_{2y}(x,0,z) = \varphi_{1x}(x,0\pm,z)(Tc_x - 1) + x\varphi_{1yy}(x,0\pm,z) - Tc\varphi_{1yy}(x,0\pm,z) + Tc_z\varphi_{1z}(x,0\pm,z) \tag{15b}$$

In Eqs. (14b) and (15b), $|z| < s(x)$, $0 \le x < 1$, where s represents the local span. This is the classical problem treated by Jones in Ref. 21. Equations (14a) and (15a) are associated with the dominance of cross flow over streamwise gradients. At a kink in the leading-edge shape such as the tip of a delta wing, this approximation will become nonuniformly valid since $\partial^2/\partial x^2$ becomes infinite at this point. To avoid such issues, only streamwise tips at the maximum span and monotonic increasing $s(x)$ are considered here. Also, only planforms symmetric in z are considered.

In this connection, there is an issue concerning the validity of the Kutta condition at the tip of cambered wings. Another concern is the assumption of a planar vortex sheet. Roll-up at downstream sections alters the planar boundary value problem to a nonplanar one.

More general planforms lead to more complex boundary value problems in the sense that the boundary conditions are mixed and depend on x through upstream interaction of the wake. For re-entrant trailing edges, the cross-flow plane is multiply connected downstream of the maximum span. The boundary value problems for such cases have been studied by other workers.

Monotonic $s(x)$ gives rise to the classical airfoil integral equation whose solution is well known (see, for example, Ref. 22).

The asymptotic behavior of φ_1 as $r = \sqrt{y^2+z^2} \to \infty$ is important for matching with the far-field outer solution and can be shown to be a doublet. Thus, if $\theta = \tan^{-1} z/y$,

$$\varphi_1 \simeq \frac{1}{2\pi}\mathfrak{D}_{11}(x)\frac{\cos\theta}{r} + \mathcal{O}\left(\frac{1}{r^3}\right) \tag{16}$$

where by a surface pressure integration, the doublet strength $\mathfrak{D}_{11}(x)$ can be shown to be proportional to the accumulated

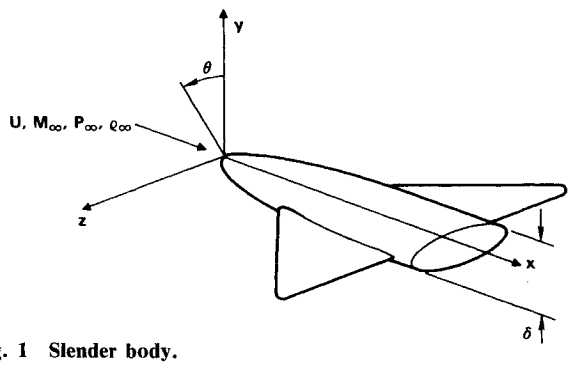

Fig. 1 Slender body.

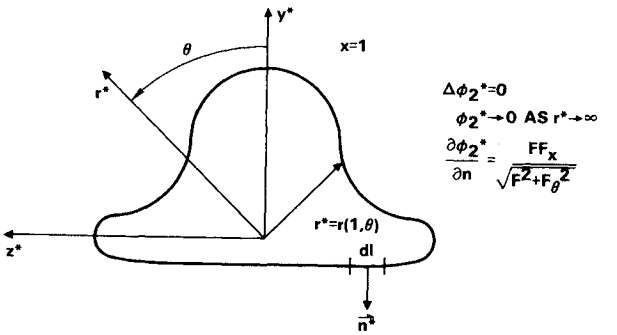

Fig. 2 Base contour cross-flow problem.

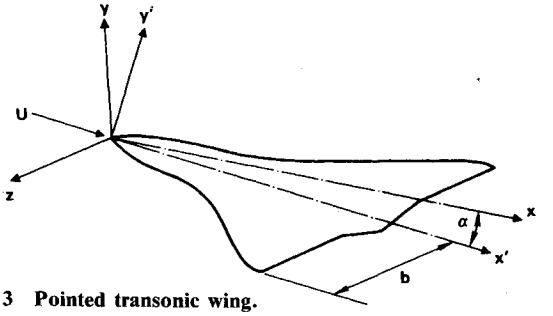

Fig. 3 Pointed transonic wing.

lift up to the station x, i.e.,

$$\mathfrak{D}_{11}(x)=2\int_{-s(x)}^{s(x)}[1-Tc_x(x,\zeta)]\sqrt{s^2-\zeta^2}\,d\zeta \tag{17}$$

For a flat wing, $c=c_x=0$ and, therefore,

$$\mathfrak{D}_{11}(x)=\pi s^2(x),\ x<1$$
$$=\pi b^2,\ x\geq 1 \tag{18}$$

Equation (16) is a key result that can be used to generate particular solutions of the Poisson equation (15a), which gives the singular behavior of φ_2 as $r\to\infty$. This behavior is an essential part of the matching to the outer transonic flow. For this matching, additional (switchback) terms are required. With these terms, the corrected form of the (matched) inner expansion is

$$\frac{\Phi}{U}=x+\alpha\varphi_1(x,y,z;K)-\alpha^2\left(\log^2\frac{1}{\sqrt{\epsilon_1}}\right)\left(\frac{\gamma+1}{16\pi^2}\right)\times\mathfrak{D}_{11}'\mathfrak{D}_{11}''(x)+\alpha^2\left(\log\frac{1}{\sqrt{\epsilon_1}}\right)[G_1(x)-\mathcal{S}_2(x)]+\alpha^2\left(\log^{1/2}\frac{1}{\sqrt{\epsilon_1}}\right)G_2(x)+\ldots \tag{19}$$

where G_1 and G_2 are determined from the $r\to 0$ limit of the outer solution, and $\mathcal{S}_2$ is evaluated from the $\tilde{r}\to\infty$ limit of the inner solution.

The outer expansion for Φ is

$$\frac{\Phi}{U}=x+\alpha^2\left(\log\frac{1}{\sqrt{\epsilon_1}}\right)\phi_1(x,\tilde{y},\tilde{z};K)+\alpha^2\left(\log^{1/2}\frac{1}{\sqrt{\epsilon_1}}\right)\phi_2(x,\tilde{y},\tilde{z};K)+\alpha^2\phi_3(x,\tilde{y},\tilde{z};K)+\ldots \tag{20}$$

where

$$\epsilon_1=\alpha_2\log\frac{1}{\sqrt{\epsilon_1}} \tag{21}$$

$$\tilde{y}=\sqrt{\epsilon_1}y,\ \tilde{z}=\sqrt{\epsilon_1}z \tag{22}$$

[Computationally, $\epsilon_1(\alpha)$ can be obtained by a functional iteration solution of the transcendental equation (21). For typical α's of interest, this process is rapidly convergent. A first guess, $\epsilon_1=-\alpha^2\log\alpha$, works well.]

Equations (20–22) lead to the following equations for ϕ_1, ϕ_2, and ϕ_3:

$$[K-(\gamma+1)\phi_{1x}]\phi_{1xx}+\phi_{1\tilde{y}\tilde{y}}+\phi_{1\tilde{z}\tilde{z}}=0 \tag{23a}$$

$$[K-(\gamma+1)\phi_{1x}]\phi_{2xx}-(\gamma+1)\phi_{2x}\phi_{1xx}+\phi_{2\tilde{y}\tilde{y}}+\phi_{2\tilde{z}\tilde{z}}=0 \tag{23b}$$

$$[K-(\gamma+1)\phi_{1x}]\phi_{3xx}-(\gamma+1)\phi_{3x}\phi_{1xx}+\phi_{3\tilde{y}\tilde{y}}+\phi_{3\tilde{z}\tilde{z}}=(\gamma+1)\phi_{2x}\phi_{2xx} \tag{23c}$$

The quantities ϕ_1, ϕ_2, and ϕ_3 contribute to the shock drag. Because of the closeness of the orders, it may be numerically important to compute all three contributions. For the purposes of this paper, only the wave drag from the asymptotically dominant term ϕ_1 will be discussed. It solves the same boundary value problem as Eq. (4), where $\mathcal{S}(x)$ is given by

$$\mathcal{S}(x)=\frac{\gamma+1}{8\pi^2}\mathfrak{D}_{11}'(x)\mathfrak{D}_{11}''(x) \tag{24}$$

instead of Eq. (5). For a flat-plate wing having monotonic increasing $s(x)$ and streamwise tips at its maximum span $\mathfrak{D}_{11}$ can be computed from Eq. (18). Thus

$$\mathcal{S}(x)=\frac{\gamma+1}{16}\left\{\frac{d}{dx}\left[\frac{d}{dx}s^2(x)\right]^2\right\} \tag{25}$$

Accordingly, the quantity $((\gamma+1)\pi)/8(d/dx)[s^2(x)]$ is directly analogous to $A(x)$. Hence, if $s'(1)=0$, we have the analogy of case (2) for the zero-lift area rule.

The wave drag D_W is, in general,

$$\frac{D_W}{\rho_\infty U^2}=-\frac{(\gamma+1)}{12}\epsilon_1^2\int\int_{\text{SHOCKS}}[\phi_{1x}]^3\,d\tilde{y}\,d\tilde{z} \tag{26}$$

where the integral represents the cumulative entropy jump across the shocks.

For $s'(1)=0$, in analogy to zero lift,

$$\frac{D_W}{\rho_\infty U^2}=-2\pi\epsilon_1^2\int_0^1\mathcal{S}(x)G_1'(x)\,dx \tag{27}$$

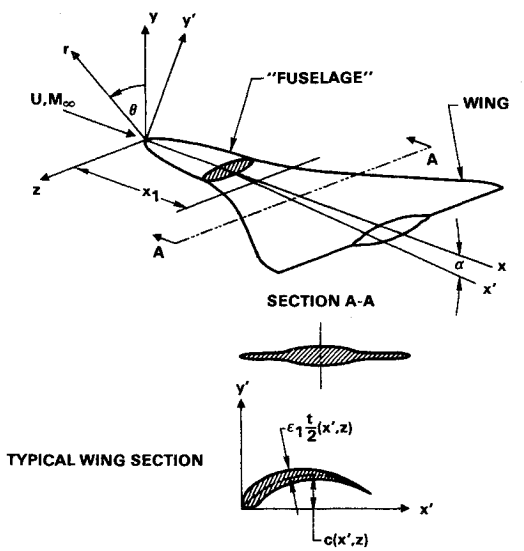

Fig. 4 Blended-wing configuration.

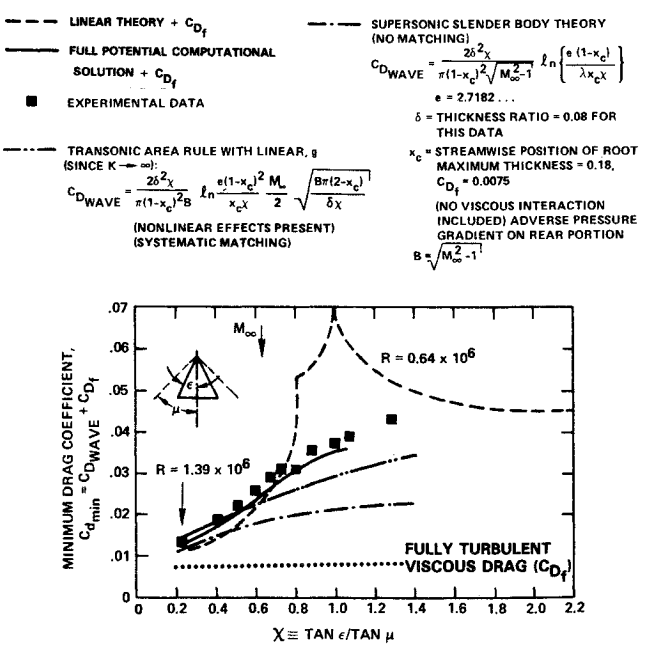

Fig. 5 Comparison of computational and analytical solutions for supersonic double-wedge delta wings, $M_\infty=1.62$.

where

$$\phi_1 \simeq \mathcal{S}(x)\ \log\bar{r} + G_1(x) + \ldots \text{ as } \bar{r}\to 0 \tag{28}$$

To summarize, the transonic small-disturbance boundary value problem for the first approximation to the shock drag due to lift of a zero-thickness wing is directly analogous to that for a body of revolution given in Eqs. (4). For the former, the "effective cross-sectional area due to lift" is proportional to $(dC_L/dx)^2$ where $C_L(x)$ is the accumulated lift up to the station x. This concept agrees with the findings of Refs. 7–11, which use a different approach.

Generalization to incorporate thickness effects has been studied by the first author. This investigation considers the generic blended wing/body configuration shown in Fig. 4, which is essentially a slender body up to station x_1. It is winglike downstream. In the body coordinates previously used, the wing/body has the representations:

$$B = r - \delta F(x',\theta) = 0,\ 0 \le x \le x_1 \tag{29a}$$

$$= y' - \alpha c(x'z) \mp \epsilon_1(\alpha)\frac{t(x',z)}{2} = 0,\ x_1 \le x \le 1 \tag{29b}$$

where c and t are, respectively, the camber and thickness functions shown in Fig. 4. The essential idea is that an additional term $\epsilon_1\varphi_{12}$ is added to the inner expansion [Eq. (13)] for the limit [Eq. (12)] to account for the thickness. Thus,

$$\frac{\Phi(x,y,z;M_\infty;\alpha)}{U} = x + \alpha\varphi_1(x,y,z;K) + \epsilon_1\varphi_{12} + \alpha^2\varphi_2 + \ldots \tag{30}$$

Substitution of Eq. (30) into the exact equations and boundary conditions leads to

$$\Delta\varphi_{12} = 0 \tag{31a}$$

and on the wing portion,

$$\varphi_{12y}(x,0\pm,z) = \pm t_x/2 \tag{31b}$$

as well as a slender-body boundary condition of the type given in Ref. 4 on the fuselage section. Since there are no forcing terms in Eq. (31a), the matching is very similar to that for the zero-thickness case. The solution of the wing cross-flow boundary value problem [Eq. (31)] is a line source across the local span, i.e.,

$$\varphi_{12} = \frac{1}{4\pi}\int_{-s}^{s} t_x(x,h)\ \log[y^2 + (z-h)^2]\,dh \tag{32}$$

The asymptotic behavior of this representation near the point at infinity is

$$\varphi_{12} \simeq \frac{1}{2\pi}\mathcal{S}_{12}\ \log r \quad \text{as } r\to\infty \tag{33a}$$

where

$$\mathcal{S}_{12} = \int_{-s}^{s} t_x(x,\zeta)\,d\zeta \tag{33b}$$

Accordingly, the only significant change in the zero thickness matching is that

$$\mathcal{S} = \mathcal{S}_{12} + \frac{(\gamma+1)}{8\pi^2}\mathcal{D}_{11}'\mathcal{D}_{11}'' \tag{34}$$

For nonplanar cross sections such as fuselages, the generalization of Eq. (33b) is

$$\mathcal{S}_{12} = \oint \frac{\partial\varphi_{12}}{\partial n}\,dl \tag{35}$$

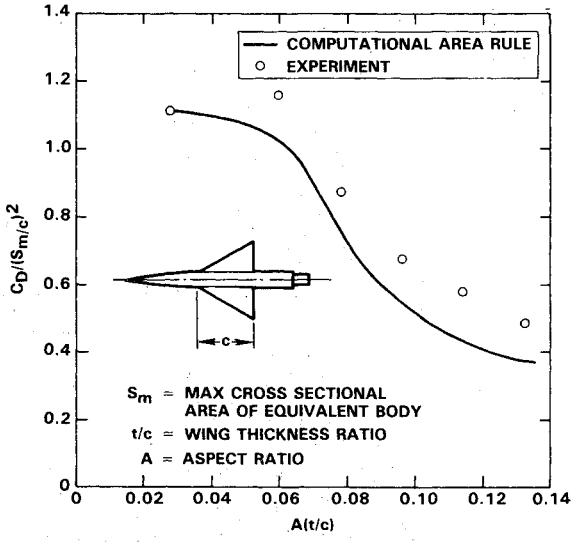

Fig. 6 Variation of predicted and experimental wave drag vs wing sweep on a missile configuration at $M_\infty = 1.4$.

where $\partial/\partial n$ is the normal to cross-sectional contour and $\oint$ signifies a line integral, which is proportional to the rate of change of cross-sectional area.

Equation (34) shows the additive effect of lift as an effective area progression to be superimposed on the geometric one. Both combine to give $\mathcal{S}(x)$, the source strength of the wave drag producing nonlinear line source governed by Eq. (23a).

Numerical Procedures

The basic methodology to computationally implement the zero-lift area rule [Eq. (7)] and its extension to lifting cases is a successive line overrelaxation (SLOR) method similar in many respects to that of Ref. 23. The SLOR process was applied to the solution of Eq. (4) to obtain $g(x;K)$ in Eq. (6). For improved accuracy, a special procedure has been developed to handle the boundary points. It regularizes the discretization in the neighborhood of the logarithmic singularity at $\bar{r}=0$ by subtracting off the singular behavior shown in Eq. (6).

Two special issues associated with the prediction of drag are the need for smoothing of the input area distribution from realistic geometries and the choice of gridding. Reference 24 contains further details on application of spline smoothing and grid clustering that helped to resolve these issues.

Results

Figure 5 shows how the supersonic asymptotic form of the nonlinear transonic theory can give substantial improvements over the linear form of supersonic slender-body theory in the moderately high supersonic regime. This figure displays the variation of the zero-lift wave drag of a double-wedge section delta wing with apex angle for freestream Mach numbers $M_\infty = 1.62$. Indicated in the figure is experimental data shown by the solid squares, taken from Ref. 25, and a full potential solution reported by Shankar.[26]

Also indicated are the linearized theory (nonslender approximation, dashed lines), linear slender-body von Kármán drag formula (dash-dot), and the supersonic asymptote of the transonic area rule (dash-double dot). The full potential theory's comparison with the experiment is excellent, whereas the linear theory's is poor. However, the extended transonic area rule provides reasonable qualitative trends useful for engineering estimates, particularly for a preliminary design basepoint definition at both Mach numbers. Much more significant is the fact that the tran-

sonic theory gives a simple closed-form solution indicated in the right side of the figure. This formula, which is not readily accessible from pure numerical solutions, shows clearly the role of all parameters, i.e., sweepback, thickness ratio, Mach number, etc., and provides the basis for optimization of these parameters for wave drag minimization. The inaccuracy of the supersonic theory is due to the "pseudotransonic" flow near the sonic ridge lines at the cusp points in the figure. A special theory designed to remedy this defect employs a nonlinear approximation in the vicinity of the leading edges and matches to the sonic line singularity of linearized theory in the far field.[27] The improvement of the supersonic limit of the transonic theory over the von Kármán formula is associated with a presumed residual nonlinear effect of the former discussed in connection with Eq. (10).

As another validation of the theory at supersonic Mach numbers, the supersonic asymptote of the nonlinear computational model is compared to experimental data from Ref. 28 in Fig. 6 for a family of missile shapes having various sweepbacks at Mach 1.4. The agreement is reasonable and the trend is correctly predicted. No attempt was made to model viscous interaction. Application of our methods to the Shuttle Orbiter in Refs. 29 and 30 indicates that crude corrections to the supersonic similarity parameter reflecting these effects improve the agreement with experiment.

For transonic Mach numbers, it is of interest to assess the usefulness of the method to predict transonic wave drag rise. For a configuration of the type considered in Fig. 6, Fig. 7 shows a comparison of the results computed by our nonlinear area rule code against experiment. This figure indicates the significance of proper modeling of wind tunnel wall effects in the code. We are using asymptotic methods to develop appropriate procedures for the transonic regime. These methods are a generalization of the procedure developed and validated in Ref. 31 for subsonic flows. Figure 7 shows that excellent agreement with experiment is obtained for a slotted wall simulation with the slot parameter $C=\frac{1}{4}$. This value was determined based on an iterative scheme at one Mach number that gave a C value in which the computations matched experiments. With this result, the calculations matched the experimental drags at all the other Mach numbers in the drag rise.

As an indicator of the applicability of the methodology to realistic aircraft geometries, Fig. 8 shows a comparison of zero-lift wave drag rise predictions with the nonlinear area rule code vs experiment for a fighter configuration. The results from two grid systems are presented. The dashed curve is for a small height computational boundary ($\bar{r}=\frac{1}{2}$) and a medium x grid. The solid curve is for a much finer x grid for the supersonic points. Also, a higher upper computational boundary ($\bar{r}_{MAX}=3$) was used with the same number of vertical nodes. Although the higher upper computational boundary reduced the average grid density, the agreement with experiment improved. Presumably, this is due to finer x grid spacing and the increased realism of the far field for $\bar{r}_{MAX}=3$ in simulating the wind tunnel wall conditions of the tests.

With validations such as that shown in Fig. 8, the nonlinear area rule is attractive as a means of design optimization of basepoint configurations typical of modern low supersonic drag shapes. These are generally low enough in aspect ratio and thickness that the assumptions of slender-body theory apply.

On the basis of the slender-body theory and nonlinear computational form of the area rule described in this paper, a drag minimization procedure was developed. This procedure is applicable to the zero-lift and lift-dominated theories described previously. This is a direct method that contrasts to the inverse procedure described in Ref. 13. The latter was used to design an EBR to support a shockless surface pressure distribution. This assumes that such a

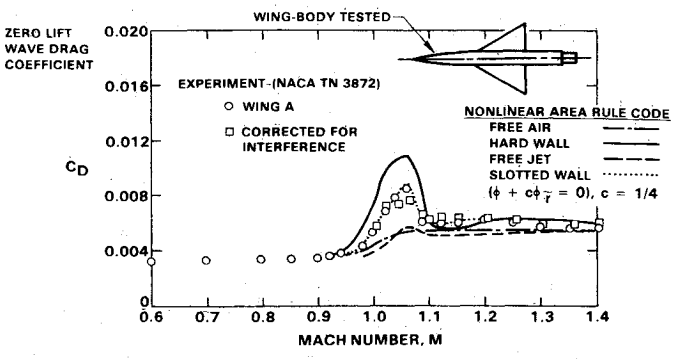

Fig. 7 Role of wind tunnel wall interference in modeling transonic wave drag rise of missile configuration.

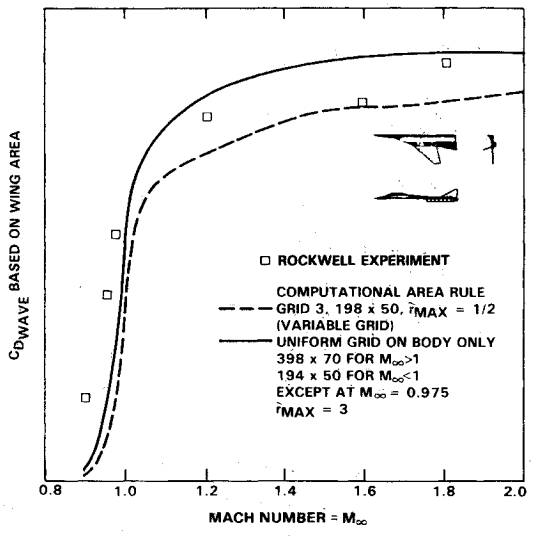

Fig. 8 Comparison of computational zero-lift drag Mach number dependence and experiment for a fighter configuration.

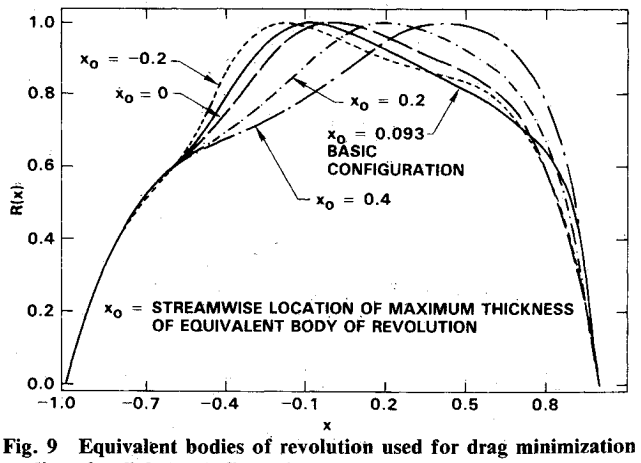

Fig. 9 Equivalent bodies of revolution used for drag minimization studies of a fighter configuration.

smoothed distribution will result in weak or nonexistent shocks off the body, and, therefore, reduced or nonexistent wave drag. Due to focusing as well as the compression wave envelope and caustic formation, however, this may not be the case and a smooth pressure distribution on the EBR may result in shocks off the body.

The method to be described deals directly with the drag and, therefore, includes the effects of shocks found off the surface. In one of our implementations, the area progression was fitted over three subintervals of the EBR length by

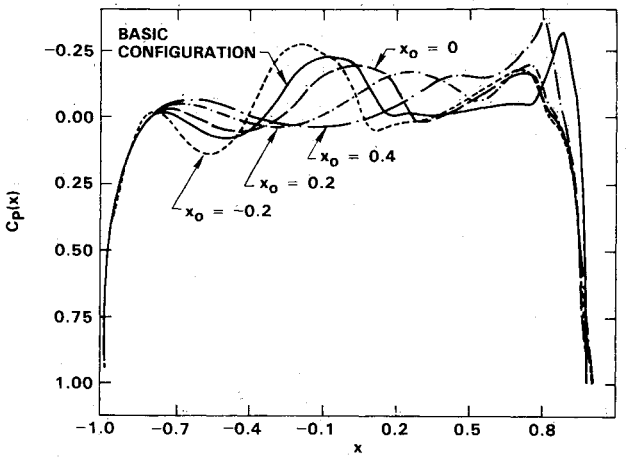

Fig. 10 Surface pressures on competing configurations, $M_\infty = 0.98$.

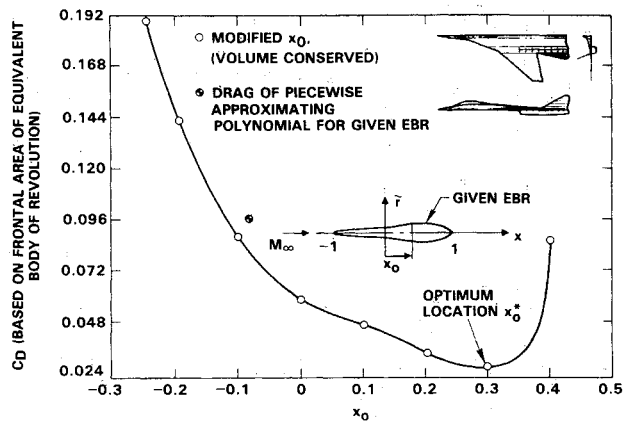

Fig. 11 Effect of modification of location of equivalent body of revolution maximum thickness (x_0) on transonic zero-lift wave drag on a fighter configuration at $M_\infty = 0.98$.

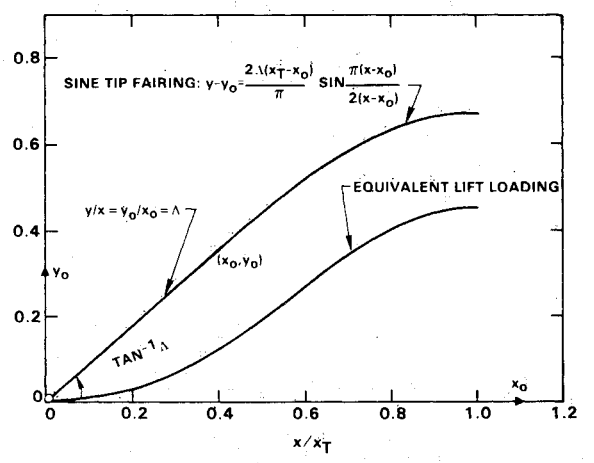

Fig. 12 Lift loading of model fighter configuration wing with sine tip fairing.

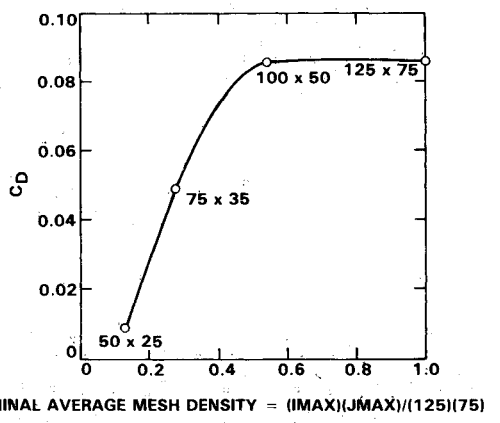

Fig. 13 Convergence of drag with respect to mesh size, $K = 64.18$, $\alpha = 11.45$ deg $= 0.2$ rad.

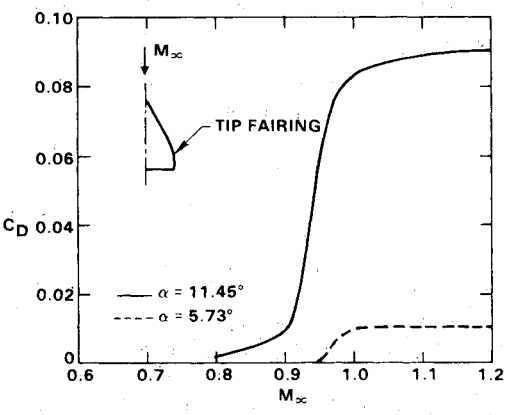

Fig. 14 Drag rise due to lift characteristics of model fighter planform, 100×50 grid, sine tip fairing.

fourth-order polynomials. Using a fixed-volume constraint, the coefficients of these polynomials were adjusted to vary the location x_0 of the maximum thickness of the EBR to minimize the zero-lift wave drag. The shapes of competing EBR configurations in the family are compared with the basic EBR of a fighter configuration in Fig. 9. Figure 10 demonstrates the surface pressure distributions for these shapes. In spite of the lack of surface shock jumps in these variations, large expansion suction spikes are evident at the rear of some of these EBRs. This drag-increasing feature can be associated with off-body shocks. The design impact of these EBR variations can be seen in Fig. 11. Here, the optimum location x_0^* at approximately 0.3 gives a wave drag reduction of nearly a factor of four from the basic level shown in the figure. This study was performed to indicate the magnitude of the reduction of levels possible. The impact of such reductions on acceleration performance can be significant. In addition, these gains can be transformed into optimum planform shaping for the lift-dominated case.

As an illustration of the lift-dominated theory, computational results will be presented for a monotonic increasing $s(x)$ planform prototype of a fighter configuration shown in Fig. 12. For uniform validity of the theory, the tip is streamwise and smooth in accord with previous remarks. Also shown is the equivalent lift loading, assuming the wing is flat.

As an indication of the convergence of the drag with respect to mesh size, Fig. 13 shows drag levels as a function of mesh density normalized to the finest mesh used. It is evident that convergence is achieved with relatively coarse grids. These combinations are compatible with operations on inexpensive mainframes.

To examine the effect of incidence on wave drag due to lift, the drag rise of the model planform is shown in Fig. 14 for two incidences. The expected dramatic rise with incidence occurs. It is evident that these levels can be appreciable when compared to induced drag. In this connection, application of the momentum theorem on a control surface surrounding the inner region shows that the φ_1 and φ_2 give only an induced drag C_{D_i}, which agrees with the classical full leading-edge suction value, under the same restrictions, i.e., for a flat-

plate wing

$$C_{D_i}/C_L^2 = 1/\mathcal{R}$$

where $\mathcal{R}$ is the aspect ratio.

Conclusions

In this paper, the application of the computational form of the nonlinear area rule to estimation and minimization of transonic wave drag has been discussed. Procedures have been outlined that offer a promise in providing reliable low-cost estimates necessary for nonlinear conceptual basepoint development. These have the additional advantages that they:

1) Avoid the computational intensity of large scale CFD codes.

2) Show applicability to the moderate supersonic regime.

3) Are suggestive of shaping concepts on the first pass that optimize and account for nonlinear effects.

4) Can provide nonlinear rather than linear lower bound targets for drag levels appropriate to the nonlinear environment.

5) Can be organized as a preliminary design user-friendly software system that can be operated on small mainframes.

6) Are based on an asymptotic approximation procedure which accounts for the nonlinear phenomena in a systematic fashion.

To achieve these goals for the lift-dominated case, additional effort is underway. This is primarily oriented toward giving a complete picture of the drag in relation to the higher-order outer approximations.

Acknowledgments

This effort was partially funded by North American Aircraft Operations (NAAO). The authors thank E. Bonner, S. White, and other NAAO personnel for useful discussions and data.

References

[1]Bonner, E., "Nonlinear Aerodynamic Wing Design," NASA CR 3950, Dec. 1985.

[2]Oswatitsch, K. and Kuene, F., "Ein Aquivalensatz fur Nichtangestellte Fluge Kleiner Spannweite in Schallnaher Stromung," *Zeitschrift fur Flugwissenshaften,* Vol. 3, No. 2, Feb. 1955, s. 29-46.

[3]Heaslet, M. and Spreiter, J. R., "Three-Dimensional Transonic Flow Theory Applied to Slender Wings and Bodies," NACA Rept. 1318, Sept. 1956.

[4]Cole, J. D., "Studies in Transonic Flow I, Transonic Area Rule-Bodies," University of California, Los Angeles, Rept. UCLA-ENG. 7257, Aug. 1972.

[5]Whitcomb, R. T., "A Study of the Zero Lift Design Drag Rise Characteristics of Wing-Body Combinations Near the Speed of Sound," NACA Rept. 1273, 1952.

[6]Jones, R. T., "Theory of Wing-Body Drag at Supersonic Speeds," NACA Rept. 1318, Sept. 1956.

[7]Cheng, H. R. and Hafez, M. M., "Transonic Equivalence Rule, A Nonlinear Problem Involving Lift," *Journal of Fluid Mechanics,* Vol. 72, Pt. 1, 1975, pp. 161-187.

[8]Cheng, H. K., "Lift Corrections to Transonic Equivalence Rule: Examples," *AIAA Journal,* Vol. 15, March 1977, pp. 366-373.

[9]Cramer, M. S., "Lifting Three-Dimensional Wings in Transonic Flow," *Journal of Fluid Mechanics,* Vol. 95, Pt. 2, Nov. 1979, pp. 223-240.

[10]Cramer, M. S., "A Note on 'Lifting Three-Dimensional Wings in Transonic Flow, by M. S. Cramer'," *Journal of Fluid Mechanics,* Vol. 109, Aug. 1981, pp. 257-258.

[11]Barnwell, R. W., "Transonic Flow About Lifting Configurations," *AIAA Journal,* Vol. 11, May 1973, pp. 764-766.

[12]Cole, J. D., "Lifting Pointed Wings in the Transonic Regime," Paper presented at U.S. National Congress of Applied Mechanics, Austin, TX, June 1986.

[13]Malmuth, N., Wu, C. C., and Cole, J. D., "Slender Body Theory and Optimization Procedures for Transonic Lifting Bodies," *Journal of Aircraft,* Vol. 21, April 1984, pp. 256-263.

[14]Sedin, Y.C.-J., "Qualitative Calculations of Transonic Drag-Rise Characteristics using the Equivalence Rule," *Proceedings of 11th International Congress of the Aeronautical Sciences,* Vol. 2, ICAS, Lisbon, Portugal, 1978, pp. 71-84.

[15]Agrell, N., Mattsson, R., and Nyberg, I., "Investigation of the Transonic Drag Rise Characteristics of Non-Slender Wing Body Combinations and Their Equivalent Axisymmetric Bodies at Zero Lift," *Proceedings of 11th International Council of the Aeronautical Sciences,* Vol. 1, ICAS, Lisbon, Portugal, 1978, pp. 292-304.

[16]Chan, Y. Y., "An Experimental Study of the Transonic Equivalence Rule with Lift," National Research Council of Canada, Aeronautical Rept. LR-609 NRC 20225, March 1982.

[17]Cole, J. D. and Cook, L. P., *Transonic Aerodynamics,* North Holland Publishing Co., Amsterdam, 1986.

[18]Ashley, H. and Landahl, M., *Aerodynamics of Wings and Bodies,* Addison-Wesley, Reading, MA, 1965, p. 116.

[19]Donovan, A. F. and Lawrence, H. R., "Aerodynamic Components of Aircraft at High Speeds," *High Speed Aerodynamics and Jet Propulsion,* Vol. VII, Princeton University Press, Princeton, NJ, 1957, p. 252.

[20]Sears, W. R. (ed.), "General Theory of High Speed Aerodynamics," *High Speed Aerodynamics and Jet Propulsion,* Vol. VI, Princeton University Press, Princeton, NJ, 1954, p. 226.

[21]Jones, R. T., "Properties of Low-Aspect Ratio Pointed Wings at Speeds Below and Above the Speed of Sound," NACA Rept. 835, 1946.

[22]Lawrence, H. R., "The Lift Distribution on Low Aspect Ratio Wings at Subsonic Speeds," *Journal of the Aeronautical Sciences,* Vol. 18, 1951, pp. 683-695.

[23]Krupp, J. A. and Murman, E. M., "Computation of Transonic Flows Past Lifting Airfoils and Slender Bodies," *AIAA Journal,* Vol. 10, July 1972, pp. 880-886.

[24]Malmuth, N., Wu, C. C., and Cole, J. D., "Transonic Wave Drag Estimation and Optimization Using the Nonlinear Area Rule," AIAA Paper 86-1798, June 1986.

[25]Love, E. S., "Investigation at Supersonic Speeds of 22 Triangular Wings Representing Two Airfoil Sections Each of 11 Apex Angles," NACA Rept. 1238, 1949.

[26]Shankar, V., "A Conservative Full Potential Implicit Marching Scheme for Supersonic Flows," *AIAA Journal,* Vol. 20, Nov. 1982, pp. 1508-1514.

[27]Schleiniger, G., "Quasi-Transonic Flow Past Delta Wings," Center for Applied Mathematics and Computation, Rensselaer Polytechnic Institute, Troy, NY, CAMAC Rept. 85-1, Nov. 1985.

[28]Page, W. A., "Experimental Determination of the Range of Applicability of the Transonic Area Rule for Wings of Triangular Planform," NACA TN-3872, 1956.

[29]Malmuth, N., Rajagopal, K., Wu, C. C., Lick, W., and Cole, J. D., "Analysis of Aerodynamic Interference on Shuttle Orbiter Transonic Airload Prediction Methodology," *Rockwell International Science Center,* Thousand Oaks, CA, Rept. SC6419-IR2, Oct. 1985.

[30]Malmuth, N., Wu, C. C., and Cole, J. D., "Slender Body Theory and Space Shuttle Transonic Aerodynamics," AIAA Paper 85-0478, Jan. 1985.

[31]Malmuth, N., "An Asymptotic Theory of Wind Tunnel Interference on Subsonic Slender Bodies," AIAA Paper 84-1625, June 1984.